Deposit Growth in the Wetting of an Angular Region with Uniform Evaporation

Rui Zheng,* Yuri O. Popov,† and Thomas A. Witten

James Franck Institute and Department of Physics,
University of Chicago, 5640 S. Ellis Ave., Chicago, Illinois 60637, USA
(Dated: February 2, 2008)

Solvent loss due to evaporation in a drying drop can drive capillary flows and solute migration. The flow is controlled by the evaporation profile and the geometry of the drop. We predict the flow and solute migration near a sharp corner of the perimeter under the conditions of uniform evaporation. This extends the study of Ref. 6, which considered a singular evaporation profile, characteristic of a dry surrounding surface. We find the rate of the deposit growth along contact lines in early and intermediate time regimes. Compared to the dry-surface evaporation profile of Ref. 6, uniform evaporation yields more singular deposition in the early time regime, and nearly uniform deposition profile is obtained for a wide range of opening angle in the intermediate time regime. Uniform evaporation also shows a more pronounced contrast between acute opening angles and obtuse opening angles.

PACS numbers: 47.55.Dz, 68.03.Fg, 81.15.-z

I. INTRODUCTION

Evaporative contact line deposition, the "coffee-drop effect", has been the subject of several recent papers [1, 2, 3, 4, 5, 6, 7, 8]. The physical problem originates from a simple phenomenon of everyday life: when a drop containing a solute such as coffee dries on a surface, the solute is driven to the contact line, forming a characteristic ring pattern. This simple phenomenon is potentially important in many areas of both scientific and industrial applications [9, 10, 11, 12]. This evaporation mechanism can create very fine lines of deposition in a robust way that requires no explicit forming. Further, it is a way of concentrating material strongly in a quantitatively predictable way. Lastly, it creates capillary flow patterns that can be useful for processing of polyatomic solutes like DNA [13, 14, 15].

One striking aspect of this deposition phenomenon is its dependence on the shape of the droplet. This dependence was recently explored by Popov and Witten [5, 6], who studied corner-shaped drops. Here the liquid region on the surface has the form of a sector of arbitrary opening angle α (Fig. 1). Such shapes contrast strongly with the circular drops treated in previous studies [1, 2, 3, 4, 8]. Popov and Witten found that this difference in shape led to striking differences in evaporative flow and deposition near the apex of the drop. Both the flow and the deposition profile showed singular power-law behavior as a function of distance r from the tip. These power laws vary in a predicted way with the opening angle, but are otherwise universal. The growth of the deposition also shows several different predicted behaviors in three defined time regimes. Thus by manip-

ulating the shape of a droplet one has extensive control over its deposition properties.

In this paper we further explore the range of control possible in evaporative deposition. This study is motivated by a finding from Ref. 6: the power laws governing the deposition depend on the evaporation conditions in the vicinity of the drop. Ref. 6 considered the usual diffusion-controlled evaporation conditions, in which the liquid is surrounded by a dry surface and the evaporation rate is limited by the diffusion of vapor away from the drop. In these conditions concentration $n(r)$ in the air obeys Laplace's equation with n at the surface set by the fixed saturation concentration. As in the analogous electrostatic problem, the gradient of n diverges at the edge and at the tip. The resulting divergent evaporation profiles contribute strongly to the controllable deposition properties found in Ref. 6.

One may readily alter these evaporation conditions, and strong differences in the deposition are expected to result. We consider a condition that contrasts strongly with the singular evaporation treated in Ref. 6, *viz. uniform* evaporation. This contrast is illustrated in Fig. 1. Uniform evaporation can be created by surrounding the drop by a wet surface instead of a dry one, as illustrated in Figure 1B. The wet-surface evaporation case allows us to discern the role of the evaporation profile in producing the power-law behaviors revealed by Ref. 6. The wet-surface evaporation case is also mathematically simpler to treat than the dry-surface case of Ref. 6. This allows us to make cleaner predictions with fewer approximations for the wet-surface case.

Our work is to a large extent a mere application of the general theory worked out in Ref. 6. We shall follow the same approach and exposition for the current case that was used in Ref. 6. Before working out the quantitative behavior we describe the experiment qualitatively. A droplet of linear dimension L is forced to have a corner shape over part of its perimeter. One may fix the edge of the drop *e.g.* by making shallow scratches in
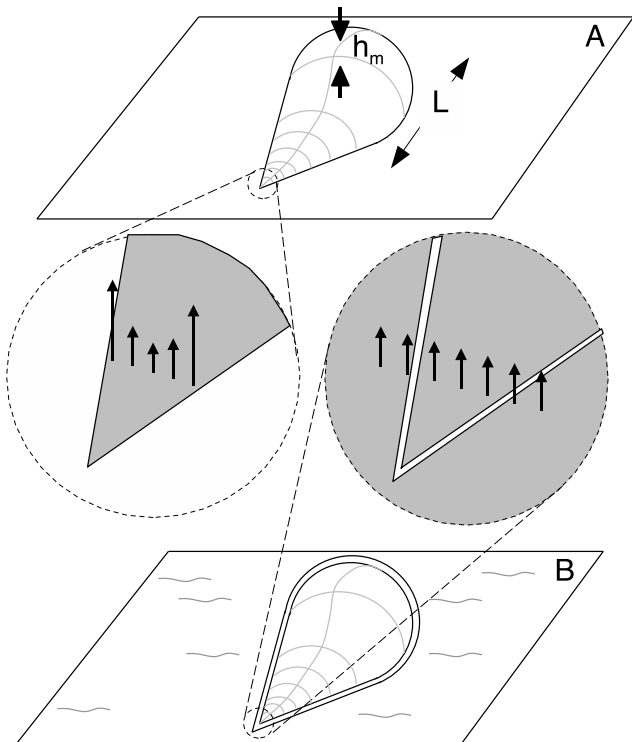
FIG. 1: Sketch of the two different evaporation conditions contrasted in the text. Both pictures show a small liquid drop of size L and maximum thickness h_m with part of its edge constrained to an angular corner shape by means of *e.g.* two scratches on the surface. Figure A shows a drop on a dry surface. Magnified tip region indicates the profile of evaporating flux across the surface by a row of arrows. Shading indicates the wet region. The flux diverges at the edges. Figure B shows a similar drop surrounded by a wet surface. Magnified region shows the uniform evaporating flux.

the surface. These serve to pin the contact line at the scratch. We choose L smaller than a few millimeters so that gravitational effects on the droplet's shape are minor. We denote the maximal thickness of the drop by h_m and keep the droplet volume small enough to assure that $h_m \ll L$. Once the evaporation starts, the volume diminishes at a constant rate, and thus h_m decreases linearly with time. At some final time t_f this thickness extrapolates to zero. Like Reference 6, we restrict our attention to time much less than this t_f, and it will show later that for $t \ll t_f$, in the early drying stages, the time dependence of L and h_m can be actually ignored. Our predictive power is strongest for this regime.

The shape of the droplet during this thinning process is dictated by its surface tension. Near the edges, the local

reduction in volume owing to thinning is much smaller than the local loss of volume to evaporation. Thus a flow towards the edge is needed in order to replace the evaporative loss. Any solute suspended in the fluid is carried along by this flow. The asymptotic flow near the tip is minimally influenced by the bulk of the drop, and thus this flow can be readily calculated. Knowing this flow profile, one may deduce how much solute should be carried to a given point on the edge in a given time t. This amount grows in a characteristic way with time and with distance from the tip. Our aim is to see how the deposition is influenced by opening angle and how much this deposition differs from the dry-surface results of Ref. 6. The main difference is in the opposite direction from what one might expect. We find that the wet-surface evaporation leads to deposition that is more concentrated at the tip than the dry-surface deposition of Ref. 6. This is despite the diverging evaporation at the edges and tip produced in the dry-surface case.

The paper is organized in parallel with Ref. 6. First, we review the basic physical model and its mathematical framework, which was introduced in Ref. 6. Next, the system is solved both analytically and numerically: the flow field is described, and its asymptotic properties studied. We obtain the power law of the deposition rate in early time regime and intermediate time regime. Then we compare our results with those of the dry-surface case. More discussion and conclusions follow in the last sections.

II. PRINCIPLES GOVERNING THE DEPOSITION

Following Ref. 5, we consider a droplet of very dilute suspension bounded in an angular region of opening angle α, as illustrated in Fig. 1. We use cylindrical coordinates (r, φ, z) defined in Fig. 2 with the range $0 < r < \infty$ and $-\alpha/2 < \varphi < \alpha/2$, to describe our system. z is the coordinate normal to the substrate. We first present the governing equations in generality and then specialize to the regime of interest: thin drops undergoing slow flows.

The equilibrium shape of the surface is dictated by the minimization of surface energy. The minimum energy surface has uniform mean curvature H. Specifically, if the surface tension of the liquid is σ and the pressure difference across the surface is Δp, then the balance of normal forces dictates:

$$\Delta p = -2H\sigma. \tag{1}$$

In the sequel, we shall represent the surface by its thickness profile $h(r, \varphi, t)$. The mean curvature H depends on the local derivatives of h, to be specified below.

As indicated in the Introduction, evaporation induces a flow towards the edge of the drop. Denoting the local velocity by $\mathbf{u}(r, \varphi, z, t)$ with in-plane component $\mathbf{u}_s$, it
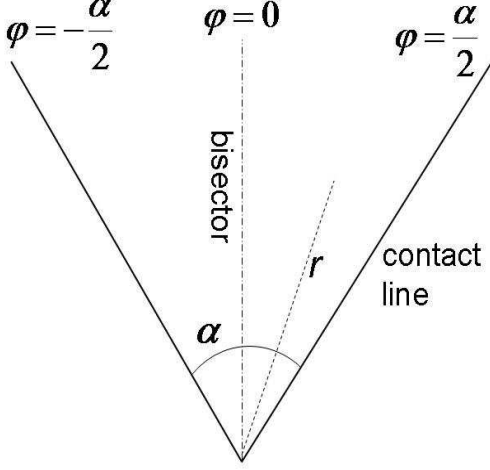
FIG. 2: Sketch of the angular drop showing geometrical quantities used in the text

is useful to define a depth-averaged velocity field $\mathbf{v}$

$$\mathbf{v} = \frac{1}{h} \int_0^h \mathbf{u}_s dz. \tag{2}$$

The condition for local mass conservation may be stated in terms of this $\mathbf{v}$:

$$\nabla \cdot (h\mathbf{v}) + \frac{J_0}{\rho}\sqrt{1 + (\nabla h)^2} + \partial_t h = 0. \tag{3}$$

Here ρ is the density of the fluid, and J_0 the mass loss per unit projected area and time at the point in question. In Ref. 6, this J_0 is a strong function of position, and it diverges at the contact line. In the present work, it is a mere constant. By itself, this condition is not sufficient to determine $\mathbf{v}$. Ultimately, $\mathbf{v}$ is determined by Newton's equations on each fluid element. We shall consider the creeping flow regime where forces are in near equilibrium and acceleration plays a negligible role in Newton's equations. Then Newton's equations reduce to the Stokes equation:

$$\nabla p = \eta \nabla^2 \mathbf{u}, \tag{4}$$

where p is the fluid pressure, and η is the dynamic viscosity. The lack of inertia implies that $\mathbf{v}$ is a potential-like flow, as shown below.

Further physical considerations and simplifications are needed to solve the system analytically. Firstly, as we are considering a thin drop, there is a separation of the vertical and horizontal scales in this problem, and several simplifications follow [6]. The pressure inside the drop p

does not depend on the z coordinate $\partial_z p = 0$. The surface of the drop should have a small slope $|\nabla h| \ll 1$. And the z-derivatives of flow dominate, i.e., $|\partial_z u_i| \gg |\partial_s u_i|$, where s represents any direction parallel to the substrate plane, and u_i refers to any velocity component. Under these considerations, (4) has the form [6]

$$\nabla_s p = \eta \partial_{zz} \mathbf{u}_s. \tag{5}$$

With boundary conditions: $\mathbf{u}_s|_{z=0} = 0, \partial_z \mathbf{u}_s|_{z=h} = 0$, we obtain

$$\mathbf{u}_s = \frac{\nabla p}{\eta}\left(\frac{z^2}{2} - hz\right). \tag{6}$$

With expressions (2) and (6), we have [6]

$$\mathbf{v} = -\frac{h^2}{3\eta}\nabla p. \tag{7}$$

Thus $\mathbf{v}/h^2$ can be represented as a gradient of the scalar potential as announced above. The flow in the drop clearly depends on the relative importance of surface forces and viscous forces. This importance is ordinarily characterized by the capillary number $Ca = v\eta/\sigma$. For water-like fluids, the capillary number is small whenever $v \ll 100$ m / s. Ordinary evaporating flows are in the range of 10^{-5} m / s; accordingly, viscous forces may be considered as weak in comparison to surface tension. Thus we anticipate that the shape of the drop is nearly the equilibrium shape in the absence of the flow. To establish this formally and systematically, we express the pressure and height as expansions in the capillary number: $p = p_0 + (Ca)p_1 + (Ca)^2 p_2 + ...$ and $h = h_0 + (Ca)h_1 + (Ca)^2 h_2 + ...$ By using these expansions in Eqs. (1), (3) and (7), we find the lowest order results [6]

$$2H = -\frac{p_0 - p_{atm}}{\sigma}, \tag{8}$$

$$\nabla \cdot (h_0^3 \nabla \psi) = -\frac{J_0}{\rho} - \partial_t h_0, \tag{9}$$

$$\mathbf{v}_0 = h_0^2 \nabla \psi, \tag{10}$$

where $\psi = -p_1(Ca)/(3\eta)$, and the leading term p_0 does not vary with local coordinates and is only a function of time t. Thus, one can use Eq. (8) to determine the equilibrium drop surface shape h_0, then solve Eq. (9) with respect to $\psi(r, \varphi, t)$, and finally determine the velocity field from Eq. (10). To simplify the notations, we will write $p_0 - p_{atm}$ as $\triangle p$, and h_0 as h in the rest of the paper.

Eq. (8) introduces a length scale into the problem, i.e., the mean radius of curvature $R(t) = \sigma/\triangle p$. Since the evaporation rate is constant in time, the droplet volume and thus its thickness decrease linearly in time until the

terminal time t_f. This means [6] that the mean curvature $R(t) \propto L^2/h_m$ can be written as

$$R(t) = \frac{R_i}{1 - t/t_f}, \qquad (11)$$

where R_i is the initial mean radius of curvature, and t_f is the total drying time. Thus in the early drying stages ($t \ll t_f$), which is the only case we are to consider in this paper, the time dependence of R can be ignored, and the shape of the drop can be assumed to vary with time adiabatically (i.e., slowly compared to all other processes). We may generally treat $R(t)$ as constant R_i in the rest of the paper, keeping in mind its time dependence (11).

III. BEHAVIOR OF THE DROP NEAR THE TIP

A. Surface shape

If written explicitly in terms of $h(r, \varphi, t)$, equation (8) reduces to the Poisson equation under the assumption of small slope of the surface:

$$\nabla^2 h = -\frac{\Delta p}{\sigma}, \qquad (12)$$

with boundary conditions $h(r, -\alpha/2) = h(r, \alpha/2) = h(0, \varphi) = 0$ [5]. Here $\sigma/\Delta p = R(t) \approx R_i$ is the mean radius of curvature, and we are only interested in the asymptotic limit $r \ll R(t)$. This problem is quite classical [17], however, its results are somewhat unexpected [5]. The leading term of the solution in the limit $r \ll R(t)$ is different for acute and obtuse angles and can be obtained by either solving the small-slope (horizontal) equation (12) or by the series expansion of the full equation (8). By both methods, the lowest order term in r of the series expansion of the surface shape h was found in Ref. 5:

$$h(r, \varphi, t) = \frac{r^\nu}{R(t)^{\nu-1}} \tilde{h}(\varphi), \qquad (13)$$

where

$$\tilde{h}(\varphi) = \frac{1}{4}\left(\frac{\cos 2\varphi}{\cos \alpha} - 1\right), \ \nu = 2, \quad 0 \le \alpha < \frac{\pi}{2}, \quad (14)$$

$$\tilde{h}(\varphi) = C(\alpha) \cos \frac{\pi\varphi}{\alpha}, \qquad \nu = \frac{\pi}{\alpha}, \ \frac{\pi}{2} < \alpha \le \pi. \quad (15)$$

Exponent ν as a function of the opening angle α is shown in Fig. 3. The acute-angle solution (13), (14) is self-similar and independent of the remote boundary condition specifying the surface shape in the bulk of the drop. The obtuse-angle solution (13), (15) has a prefactor $C(\alpha)$, which does depend on the remote boundary condition in the bulk of the drop [17] and has the form [5]:

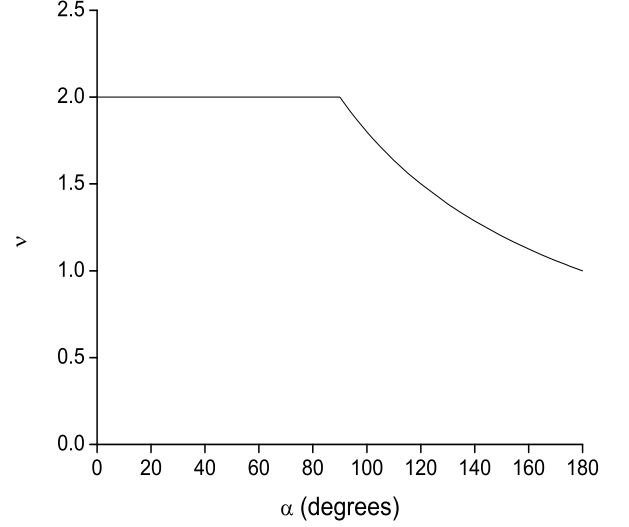$$C(\alpha) = \frac{1}{4\alpha - 2\pi} + C_0 + O\left(\alpha - \frac{\pi}{2}\right), \qquad (16)$$

FIG. 3: Relation between the exponent ν and the opening angle α

where C_0 is *independent* of α and is determined by the remote boundary condition. Clearly, the leading-order solution (13), (14), and (15) diverges when α approaches the right angle from either side.

The notable difference between acute and obtuse opening angles in the main order results (13), (14), and (15) was first discussed in Ref. 17. For acute opening angles, a *local similarity* solution is valid, i.e., the solution that has no arbitrary coefficients and is independent of the remote boundary conditions in the bulk of the drop that need to be further prescribed. Physically, the surface shape of the drop near the tip is controlled locally and is independent of the physical conditions far from the tip. For obtuse opening angles, however, the local similarity does not hold, and the surface shape is no longer controlled locally. Accordingly, the coefficient $C(\alpha)$ depends on the remote boundary conditions. This contrast between acute and obtuse opening angles leads to different flow behavior and different deposition properties as will be shown later.

The dependence of $C(\alpha)$ on the remote boundary condition can be illustrated in the following way. $C(\alpha)$ can be expressed in terms of the linear dimension L and the maximal thickness h_m, which characterize the global shape of the drop. Along the bisector $\varphi = 0$, let $r \rightarrow L$ and $h \rightarrow h_m$, and using approximation $R(t) \approx R_i \propto L^2/h_m$, one can obtain from Eqs. (13) and (15):

$$C(\alpha) \propto \left(\frac{L}{h_m}\right)^{\nu-2}. \qquad (17)$$

Clearly, $C(\alpha)$ is small since $\nu < 2$ for obtuse opening angles, and its time dependence is weak in the early drying

stages and can be ignored.

For numerical purposes, C_0 in (16) will be set to unity, as was done in Ref. 6. This is justified by the fact that when α approaches $\pi/2$ from above, the divergent term $1/(4\alpha - 2\pi)$ dominates, and the properties of the system become independent of C_0. In the opposite limit, $\alpha = \pi$, the tip of the angular region can be chosen at any point on the contact line due to the symmetry, and physical properties of the drop are again independent of C_0. Although for arbitrary obtuse opening angle C_0 is controlled by the remote boundary conditions, numerical studies have shown consistent results that did not vary substantially with C_0.

The special case $\alpha = \pi/2$ invites further explanation. According to expressions (14) and (15), function $\tilde{h}(\varphi)$ diverges when α approaches $\pi/2$ from either side. This divergence is artificial, however [5]. This issue is explained in some detail in Appendix B. In the rest of the work, we will treat $\alpha = \pi/2$ as the limiting case and will keep in mind the possible divergence of expressions (14) and (15).

B. Reduced pressure

Now we are ready to solve Eq. (9). We are interested only in the asymptotic behavior when $r \to 0$ (or $r \ll R$), and in this limit $\partial_t h \propto r^\nu$ as we know from Eq. (13). Thus, $\partial_t h$ can be safely dropped compared to the constant term J_0/ρ on the right-hand side of Eq. (9). Physically, in this asymptotic limit during the early drying stages the fluid mass transport due to the gradient of the flow flux is uniquely balanced by the evaporation from the surface locally at each moment, with the mass change brought about by the local height change being a higher order small quantity that can be ignored.

The asymptotic solution for the reduced pressure $\psi(r, \varphi, t)$ of Eq. (9) can be expressed as:

$$\psi(r, \varphi, t) = \frac{J_0}{\rho} \frac{r^{2-3\nu}}{R(t)^{3-3\nu}} \tilde{\psi}(\varphi), \qquad (18)$$

where the exponent of r is determined by simply counting the powers of r on the left side of Eq. (9). From Eqs. (9) and (18), we find explicitly the differential equation that $\tilde{\psi}(\varphi)$ should satisfy [6]

$$\frac{d^2\tilde{\psi}}{d\varphi^2} + \frac{3}{\tilde{h}} \frac{d\tilde{h}}{d\varphi} \frac{d\tilde{\psi}}{d\varphi} - 2(3\nu - 2)\tilde{\psi} = -\frac{1}{\tilde{h}^3}. \qquad (19)$$

This equation depends implicitly on the opening angle, as $-\alpha/2 \leq \varphi \leq \alpha/2$, with ν and $\tilde{h}$ depending on α as shown in Eqs. (14) and (15).

The boundary conditions associated with Eq. (19) need to be clarified. Firstly, we expect the flow field to be totally symmetrical with respect to the bisector $\varphi = 0$, and therefore $\tilde{\psi}$ should be even in φ:

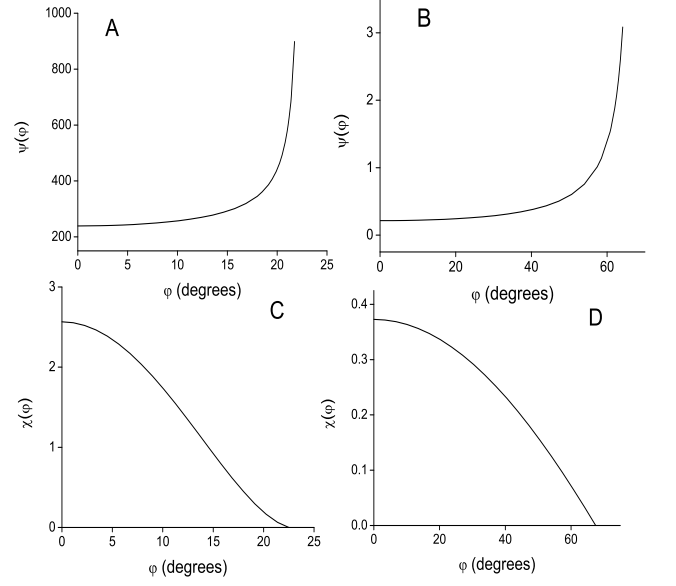$$\left. \frac{d\tilde{\psi}}{d\varphi} \right|_{\varphi=0} = 0. \qquad (20)$$

FIG. 4: A, B: The reduced pressure function $\tilde{\psi}(\varphi)$ for representative acute and obtuse opening angles. A: $\alpha = \pi/4$, B: $\alpha = 3\pi/4$; C, D: The regularized function $\tilde{\chi}(\varphi)$, defined in Appendix A as $\tilde{\chi}(\varphi) = \tilde{h}^2 \tilde{\psi}(\varphi)$, corresponding to A and B

Secondly, the outer boundary condition at $\varphi = \alpha/2$ can be identified explicitly as

$$\left. \tilde{h}^3 \frac{d\tilde{\psi}}{d\varphi} \right|_{\varphi=\alpha/2} = 0. \qquad (21)$$

In Appendix A, we justify this boundary condition, and discuss how Eq. (19) may be regularized.

The boundary problem of Eq. (19) with boundary conditions (20) and (21) is complete and has a unique solution. We show the numerical solutions $\tilde{\psi}(\varphi)$ for typical opening angles $\alpha = \pi/4$ and $3\pi/4$ in Fig. 4. The analytical solution to this boundary problem and its asymptotics are also discussed in Appendix A.

Eq. (19) is solvable analytically for special opening angle $\alpha = \pi$. If written in terms of the Cartesian coordinates (where the x axis is the contact line and the y axis is the bisector), the reduced pressure function ψ can be found from Eqs. (15), (18), and (19), and has the form

$$\psi = \frac{J_0}{\rho} \frac{1}{C^3(\pi)} \frac{1}{y}. \qquad (22)$$

Since is does not depend on x, this result is fully consistent with the symmetry of the system when $\alpha = \pi$.

For $0 \leq \alpha < \pi$, no special angle exists to reduce the complexity of the equation. Angle π is the only opening angle where we can obtain analytic results in a closed

form. For $\alpha = \pi$ the simplicity is well anticipated, since this limiting case has no apex at all. Without an apex, all points on the boundary are equivalent, and most of the resulting properties follow by symmetry. We will use the exact solution at the opening angle π to test our numerical results and analytical asymptotics.

IV. RESULTS FOR THE PHYSICAL PROPERTIES OF THE SYSTEM

A. Flow field

In polar coordinates, the velocity field (10) can be expressed explicitly:

$$\mathbf{v} = v_r \hat{r} + v_\varphi \hat{\varphi}, \qquad (23)$$

$$v_r = -(3\nu - 2)\frac{J_0}{\rho}\left(\frac{r}{R(t)}\right)^{1-\nu}\tilde{h}^2\tilde{\psi}, \qquad (24)$$

$$v_\varphi = \frac{J_0}{\rho}\left(\frac{r}{R(t)}\right)^{1-\nu}\tilde{h}^2\frac{d\tilde{\psi}}{d\varphi}. \qquad (25)$$

As we assume that solute particles carried by the fluid move with the same velocity as the flow itself (this assumption was actually confirmed both theoretically and experimentally, and a theoretical estimate can be found in [16]), the trajectory of each particle is identified as the streamline of the flow field, and can be obtained by integrating the velocity field [6]:

$$\frac{dr}{rd\varphi} = \frac{v_r}{v_\varphi} = -(3\nu - 2)\tilde{\psi}\left(\frac{d\tilde{\psi}}{d\varphi}\right)^{-1}. \qquad (26)$$

If the particle eventually arrives at $(r_0, \alpha/2)$ on the contact line, the trajectory reads as [6]

$$r(\varphi) = r_0 \exp\left((3\nu - 2)\int_\varphi^{\alpha/2}\tilde{\psi}\left(\frac{d\tilde{\psi}}{d\varphi'}\right)^{-1}d\varphi'\right). \qquad (27)$$

In Fig. 5 we show the flow field configuration for the opening angle $\alpha = \pi/2$ computed numerically with the acute-angle expression (14).

These flow trajectories are independent of the dimensional quantities like the evaporation rate J, and they depend only on the opening angle [6]. Thus, the trajectory of the moving solute particle does not depend on how fast the drop evaporates and how thin the liquid layer is.

We now consider the asymptotic properties of the streamlines. For $\varphi \to \alpha/2$, velocity component v_r vanishes due to the outer boundary condition, which amounts to the statement that no mass flows inward or outward along the contact line, while component v_φ remains finite due to the asymptotic behavior of $d\tilde{\psi}/d\varphi$
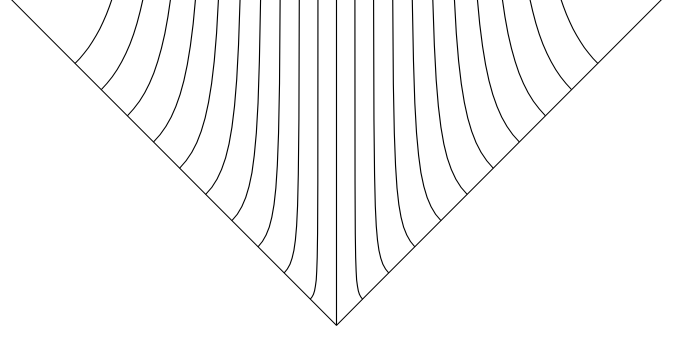

FIG. 5: Streamline configuration for the opening angle $\pi/2$

(A11), and goes as

$$v_\varphi \to \frac{J_0}{\rho}\left(\frac{r}{R(t)}\right)^{1-\nu}\left|\frac{d\tilde{h}}{d\varphi}\left(\frac{\alpha}{2}\right)\right|^{-1}, \qquad (28)$$

or, if written explicitly by employing results (14) and (15),

$$v_\varphi \to \frac{2J_0}{\rho}\frac{1}{\tan\alpha}\left(\frac{r}{R(t)}\right)^{-1} \qquad 0 \le \alpha < \frac{\pi}{2},$$

$$v_\varphi \to \frac{J_0}{\rho}\frac{\alpha}{\pi C(\alpha)}\left(\frac{r}{R(t)}\right)^{1-\pi/\alpha} \qquad \frac{\pi}{2} < \alpha \le \pi. \qquad (29)$$

In particular, v_φ seemingly vanishes as $\alpha \to \pi/2$. However, in fact it does not. We explore this point in Appendix B. Consequently, as $\varphi \to \alpha/2$, $dr/d\varphi \to 0$, and the streamlines are perpendicular to the contact line.

In the opposite limit, $\varphi \to 0$, the streamlines reach far into the bulk of the drop, and function $r(\varphi)$ is divergent.[1] Behavior of the streamlines depends on the asymptotic properties of $\tilde{\psi}$ near the bisector, which, according to Eq. (19) and boundary condition (20), can be written as

$$\tilde{\psi} \to \tilde{\psi}(0) + \frac{1}{2}\left(2(3\nu - 2)\tilde{\psi}(0) - \frac{1}{\tilde{h}^3(0)}\right)\varphi^2. \qquad (30)$$

The boundary value $\tilde{\psi}(0)$ requires the complete solution of Eq. (19). The divergent part of the integration in (27) is then uniquely determined by the asymptotic form (30) since (Eq. (50) in Ref. 6):

$$\int_\varphi^{\alpha/2}\tilde{\psi}\left(\frac{d\tilde{\psi}}{d\varphi'}\right)^{-1}d\varphi' \to \frac{1}{2(3\nu - 2) - \kappa^2}\ln\frac{\alpha}{2\varphi}, \qquad (31)$$

where

$$\kappa^2 = \frac{1}{\tilde{h}^3(0)\tilde{\psi}(0)}. \qquad (32)$$

---

[1] Since $\mathbf{v}/h^2$ is a potential flow, the streamlines $r(\varphi)$ may end only where the reduced pressure ψ assumes local extreme values, i.e., at the contact line and at infinity (in the bulk of the drop).

Therefore the streamlines in this limit scale as

$$r \to r_0 \left(\frac{\alpha}{2\varphi}\right)^\epsilon, \qquad \varphi \to 0, \tag{33}$$

with

$$\epsilon = \frac{3\nu - 2}{2(3\nu - 2) - \kappa^2}, \tag{34}$$

and $r_0 = r(\alpha/2)$ is the contact line distance.

For special opening angle π, it is straightforward to obtain the streamline equation and the velocity components in terms of Cartesian coordinates from Eqs. (22), (24), and (25):

$$x = r_0 \tag{35}$$

$$v_x = 0, \quad v_y = -\frac{1}{C(\pi)} \frac{J_0}{\rho}. \tag{36}$$

Accordingly, we have $\kappa^2(\pi) = 1$ and $\epsilon(\pi) = 1$. The streamline configuration and velocity are fully consistent with the symmetry of the system, since the position of the apex is no longer well defined when $\alpha = \pi$.

We do not have exact analytic results for exponents $\kappa^2(\alpha)$ and $\epsilon(\alpha)$ for arbitrary opening angle α, since equation (19) can not be solved in closed form to obtain $\tilde{\psi}(0)$. One has to solve the boundary value problem (A13) numerically to fix $\tilde{\psi}(0)$, and determine κ^2 and ϵ in terms of the opening angle α. We show the dependence of κ^2 and ϵ on the opening angle α in Figs. 6 and 7; for comparison, we also include results found in Ref. 6 for the case of dry-surface evaporation. Numerical results are in agreement with the analytic result we have found for the special case $\alpha = \pi$.

The exponent ϵ determines the asymptotic behavior of the streamlines near the bisector $\varphi = 0$. According to Eq. (33), the distance between a streamline and the bisector scales with φ as $\varphi r(\varphi) \propto \varphi^{1-\epsilon}$ in this limit. As is apparent in Fig. 7, in the case of wet-surface evaporation ϵ is equal to unity for $\alpha = \pi/2$ and π, and hence $\varphi r(\varphi)$ remains constant asymptotically. Geometrically, this means that streamlines run parallel to the bisector when $\varphi \to 0$. This result also follows directly from our analytic solution (35) for $\alpha = \pi$ and from Fig. 5 for $\alpha = \pi/2$. For $\alpha = \pi$ this geometric property of streamlines is well anticipated from the symmetry of the system; for $\alpha = \pi/2$, however, it is not obvious. For acute opening angles, we find $\epsilon < 1$, and therefore the asymptotic distance decreases when $\varphi \to 0$, and the streamlines converge toward the bisector as $r \to \infty$. The incoming particles are moving along the trajectory away from the bisector. For obtuse opening angles, we have $\epsilon > 1$, and therefore the asymptotic distance increases when $\varphi \to 0$, and the streamlines diverge away from the bisector as $r \to \infty$. Now the incoming particles first move along the trajectory toward the bisector, reach a minimal distance,

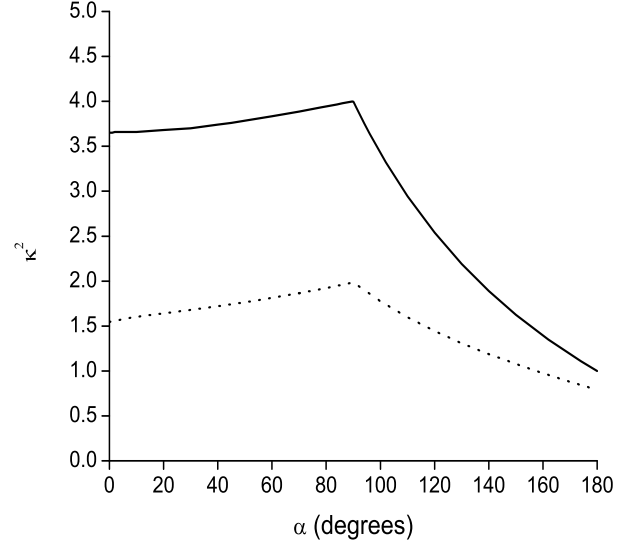FIG. 6: Dependence of parameter κ^2 on opening angle α. The solid line corresponds to the case of uniform evaporation. The dotted line, obtained in Ref. 6, corresponds to the dry-surface evaporation with quadratic profile (Eq. (25) in Ref. 6).

FIG. 7: Dependence of the stream line asymptotic exponent ϵ (when $\varphi \to 0$) on the opening angle α. The solid line corresponds to the uniform evaporation case. The dotted line, obtained in Ref. 6, corresponds to the dry-surface evaporation with quadratic profile (Eq. (25) in Ref. 6).
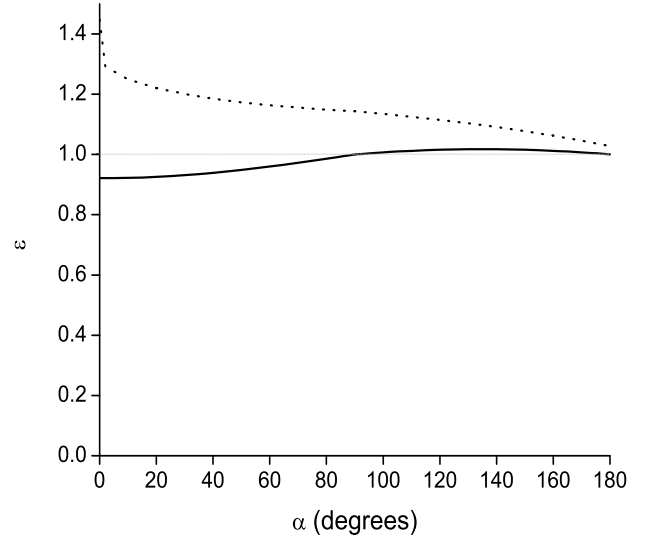
and then turn away toward the contact line. For dry-surface evaporation [6], streamlines always diverge away from the bisector, since $\epsilon > 1$ in this case for all opening angles (Fig. 7).

B. Solute transfer and deposit growth

As in the dry-surface evaporation case (Eqs. (55) and (56) in Ref. 6), one can now calculate the time it takes for the solute particles initially located at (r, φ) (where $0 \leq \varphi \leq \alpha/2$) to move along the streamline to the contact line $(r_0, \alpha/2)$. We use Eqs. (25) and (27) to write:

$$t = \int_{\varphi}^{\alpha/2} \frac{r d\varphi}{v_{\varphi}} \tag{37}$$

$$= t_0 \int_{\varphi}^{\alpha/2} \frac{\exp\left(\nu\left(3\nu - 2\right) \int_{\varsigma}^{\alpha/2} \tilde{\psi}\left(\xi\right) \left(\frac{d\tilde{\psi}}{d\xi}\right)^{-1} d\xi\right)}{\tilde{h}^2 \frac{d\tilde{\psi}}{d\varsigma}} d\varsigma,$$

where

$$t_0 = \frac{\rho}{J_0} \frac{r_0^{\nu}}{R(t)^{\nu-1}} \rightarrow \frac{\rho}{J_0} \frac{r_0^{\nu}}{R_i^{\nu-1}} \tag{38}$$

is a combination of the system parameters that has a dimension of time. In the early stages of the drying process, we can approximate $R(t)$ by R_i, and t_0 is therefore independent of time. For each streamline indexed by contact line distance r_0, and for each time t, there exists a unique $\varphi(r_0, t)$ determined by Eq. (37), such that all the solute located in the area bounded by neighboring streamlines indexed by r_0 and $r_0 + dr_0$ in the domain $\varphi(r_0, t) \leq \varsigma \leq \alpha/2$ reaches the contact line and becomes part of the deposit within time t. Let us denote the mass accumulated between r_0 and $r_0 + dr_0$ at the contact line by time t as $dm(r_0, t)$.

To study solute transfer and deposit growth, we want to understand the deposit distribution along the contact line, as well as its growth rate with time. We can consider the amount of solute $d(dm)/dt$ arriving at the contact line during time dt through the flow tube bounded by neighboring streamlines indexed by r_0 and $r_0 + dr_0$, as shown in Figure 8 (compared to Ref. 6, where a global approach was employed, and the integral quantity with respect to time dm was computed). If we assume that the initial concentration of the solute is constant c_0 everywhere in the drop, then $d(dm)/dt$ can be expressed as:

$$\frac{d(dm)}{dt}(r_0, t) = c_0 h(\vec{r}(r_0, \varphi(r_0, t))) |\vec{v}(\vec{r}) \times d\vec{r}|. \tag{39}$$

Again, we can start with the special opening angle π, for which analytical results can be obtained straightforwardly. In Cartesian coordinates, the surface shape (15) reads as $h = C(\pi)y$, the velocity is given by Eq. (36), and $y = v_y t$. Expression (39) can be simplified as

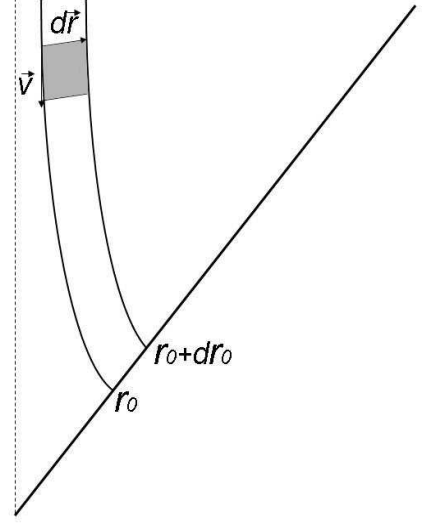$$\frac{d(dm)}{dt}(r_0, t) = c_0 h(\vec{r}(r_0, \varphi(r_0, t))) |v_y| dr_0, \tag{40}$$

FIG. 8: Qualitative sketch of the local approach. The solute in the shaded area will be arriving at the contact line through the flowtube at time t, and this corresponds to $d(dm/dt)(r_0, t)$.

from where a power law can be found:

$$\frac{d}{dt}\left(\frac{dm}{dr_0}\right) = \frac{c_0}{C(\pi)} \left(\frac{J_0}{\rho}\right)^2 t. \tag{41}$$

The deposition rate for $\alpha = \pi$ does not depend on r_0, which is anticipated, since the position of the apex is no longer well defined. Thus, for $\alpha = \pi$ there is a unique power law in the whole domain of φ and for all times t in the early drying stages.

For arbitrary opening angles α other than π, however, the deposition rate can not be calculated analytically without knowledge of the closed form of $\tilde{\psi}(\varphi)$. Instead, we have to analyze (37) as well as other relevant quantities asymptotically in two different limiting cases: $\varphi \rightarrow 0$ and $\varphi \rightarrow \alpha/2$. These two different asymptotic regions correspond to two different time regimes, when the deposition rate follows different power laws, as was first introduced in Ref. 6:

early time regime: $t \ll t_0$, when only solute particles initially located near the boundary can reach the contact line and become part of the deposit. Properties of deposition in the time regime are governed by the asymptotic $\varphi \rightarrow \alpha/2$.

intermediate time regime: $t_0 \ll t \ll t_f$, when solute particles initially located near the bisector are able to reach the contact line. This time regime is governed by the limit $\varphi \rightarrow 0$. The condition $t \ll t_f$, where t_f is the total drying time, means that we are still considering early enough drying stages, where our model applies.

As argued in Ref. 6, the separation of two time regimes

works worse when the opening angle α increases toward π. This can be readily seen in our case: as shown in (41), the deposition rate follows the same power law throughout the early drying stages when $\alpha = \pi$, and the two time regimes are indistinguishable.

1. Deposit growth in the early time regime

In the early time regime, only the solute particles initially located near the contact line contribute to the mass deposition.

As shown earlier, the velocity component v_r vanishes in the limit $\varphi \to \alpha/2$, and streamlines are perpendicular to the contact line. Expression (39) has a very simple form:

$$\frac{d(dm)}{dt} \propto v_\varphi h dr_0, \qquad \varphi \to \frac{\alpha}{2}. \tag{42}$$

In this limit, the asymptotic forms are $h \propto r_0^\nu(\alpha/2 - \varphi)$ (Eq. (13)), $v_\varphi \propto r_0^{1-\nu}$ (Eq. (25)), and $t(\varphi) \propto r_0^\nu(\alpha/2-\varphi)$ (Eq. (37)), and therefore Eq. (42) can be written in the form of a power law:

$$\frac{d}{dt}\left(\frac{dm}{dr_0}\right) \propto t r_0^\beta, \tag{43}$$

where

$$\beta = 1 - \nu. \tag{44}$$

One can also use the approach employed in Ref. 6 to find the power law of the deposition rate (compared to Eq. (60) in Ref. 6):

$$\frac{dm}{dr_0}(r_0, t) \propto t^2 r_0^\beta, \tag{45}$$

where β is again given by (44), which is in agreement with result (43) and the result we found for special angle π (41). The dependence of the exponent β on the opening angle is shown in Fig. 9, where the exponent obtained in Ref. 6 for the case of dry-surface evaporation is also included for comparison.

The relation (44) can be understood in the following way. Let δ be the distance from the contact line. When δ is small, mass conservation demands $h\mathbf{v} \propto J\delta$, and hence $\mathbf{v} \propto (dh/d\delta)^{-1}$, i.e., near the contact line the velocity should be inversely proportional to the slope of the drop surface $|dh/d\delta|$. According to (13), near the contact line $h = r^\nu \tilde{h}(\varphi) \approx r^\nu \tilde{h}(\alpha/2 - \delta/r)$, and $|dh/d\delta| \propto r^{\nu-1}\left.(d\tilde{h}/d\varphi)\right|_{\varphi=\alpha/2}$. Therefore, the velocity is proportional to $r^{1-\nu}$, so is the mass deposition rate, and Eq. (44) follows.

2. Deposit growth in the intermediate time regime

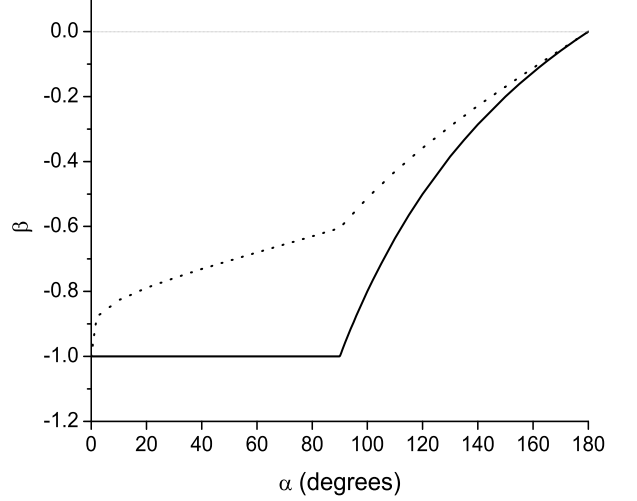In the intermediate time regime, we need again to find the power law of $d(dm)/dt$. By analyzing expressions

FIG. 9: Dependence of the exponent β of the contact line distance r_0 on the opening angle α in the power law dm/dr_0 (Eq. (45)) in the early time regime. The solid line corresponds to the uniform evaporation, and the dotted line corresponds to the dry-surface evaporation with the quadratic profile (Eq. (25) in Ref. 6).

(13), (24), (25), (33), and (37) in the limit $\varphi \to 0$, we find that relevant physical quantities assume the following asymptotic forms:

$$r \propto r_0 \varphi^{-\epsilon}, \qquad h \propto r_0^\nu \varphi^{-\nu\epsilon}, \tag{46}$$

$$v_r \propto -r_0^{1-\nu}\varphi^{-\epsilon(1-\nu)}, \qquad v_\varphi \propto r_0^{1-\nu}\varphi^{1-\epsilon(1-\nu)}, \tag{47}$$

$$t \propto r_0^\nu \varphi^{-\nu\epsilon}. \tag{48}$$

Then, according to Eq. (39),

$$\frac{d(dm)}{dt} \propto h\,|\vec{v}(\vec{r}) \times d\vec{r}| = h\,|v_\varphi dr - v_r r d\varphi|\,. \tag{49}$$

By assuming $dt = 0$ along the direction of $d\vec{r}$, we can derive the relation $d\varphi \propto -(\varphi/r_0)\,dr_0$ from Eq. (48). Using Eqs. (46) and (47), expression (49) can be simplified as:

$$\frac{d}{dt}\left(\frac{dm}{dr_0}\right) \propto r_0 \varphi^{1-2\epsilon}. \tag{50}$$

Together with (48), we finally obtain:

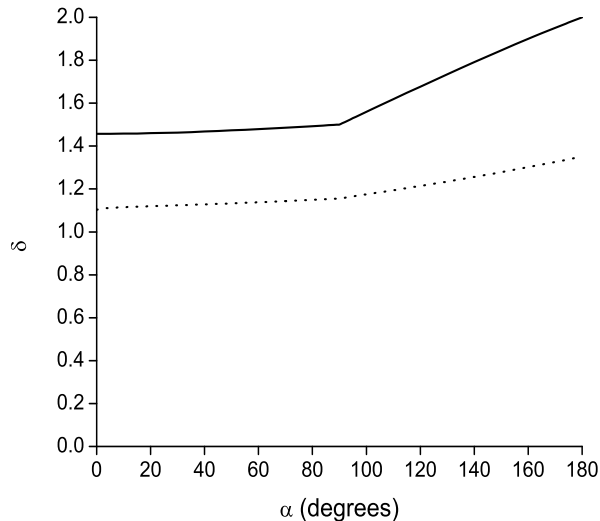$$\frac{d}{dt}\left(\frac{dm}{dr_0}\right) \propto t^{\delta-1} r_0^\gamma, \tag{51}$$

FIG. 10: Dependence of the exponent δ of time t on the opening angle α in the power law dm/dr_0 (Eq. (54)) in the intermediate time regime. The solid line corresponds to the uniform evaporation, and the dotted line corresponds to the dry-surface evaporation with the quadratic profile (Eq. (25) in Ref. 6).

FIG. 11: Dependence of the exponent γ of the contact line distance r_0 on the opening angle α in the power law dm/dr_0 (Eq. (54)) in the intermediate time regime. The solid line corresponds to the uniform evaporation, and the dotted line corresponds to the dry-surface evaporation with the quadratic profile (Eq. (25) in Ref. 6).

where

$$\delta = 1 + \frac{\kappa^2}{\nu\,(3\nu - 2)} \tag{52}$$

and

$$\gamma = 1 - \frac{\kappa^2}{3\nu - 2}. \tag{53}$$

In this limit, we can also follow Ref. 6 to compute the power law of dm/dr_0, and we find the deposition rate to be (compared to Eq. (63) in Ref. 6):

$$\frac{dm}{dr_0}(r_0, t) \propto t^\delta r_0^\gamma, \tag{54}$$

with the same scaling exponents given by (52) and (53). Again Eqs. (51) and (54) are in agreement with each other and exponents (52) and (53) are in agreement with the values of exponents we obtained for special angle π. We show the dependence of the exponents δ and γ on the opening angle in Figs. 10 and 11, where we also include results of Ref. 6 for comparison.
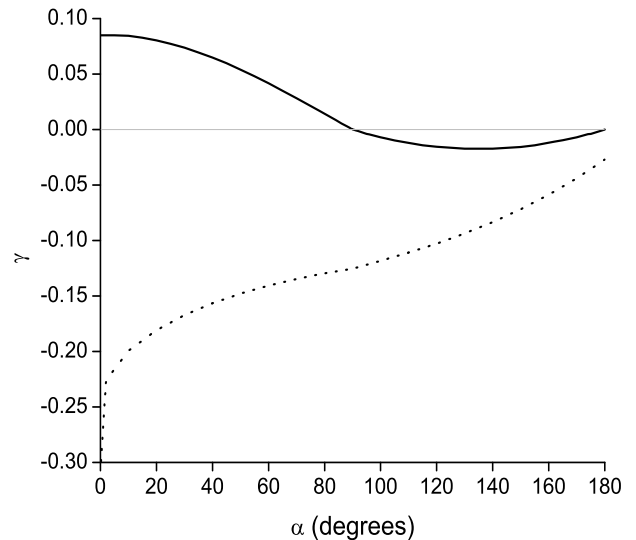
V. COMPARISON WITH THE DRY-SURFACE EVAPORATION CASE

Popov and Witten [6] considered a general evaporation rate $J(r, \varphi)$ of the asymptotic form

$$J \to r^{\mu-1}\left(\frac{\alpha}{2} - |\varphi|\right)^{-\lambda}, \qquad |\varphi| \to \frac{\alpha}{2}. \tag{55}$$

The wet-surface case considered here corresponds to $\mu = 1$ and $\lambda = 0$. The results of the previous section may be obtained by setting $\mu = 1$ and $\lambda = 0$ in the general expressions of Ref. 6. In some cases this limit permits simpler expressions and more explicit solutions as we have seen. For the dry-surface evaporation case studied in Ref. 6, $\lambda = 1/2$ and μ is an explicit function of the opening angle α (Fig. 12) reflecting the singular behavior of the Laplacian vapor concentration field [18]. Compared to the dry-surface evaporation, the uniform evaporation rate yields different deposition properties in both early and intermediate time regimes.

A. Early time regime

In this regime, only the asymptotic form (55) of the evaporation rate J when φ approaches $\pm\alpha/2$ matters. While μ is relevant to the dependence of the reduced pressure function ψ on coordinate r, the exponent λ governs
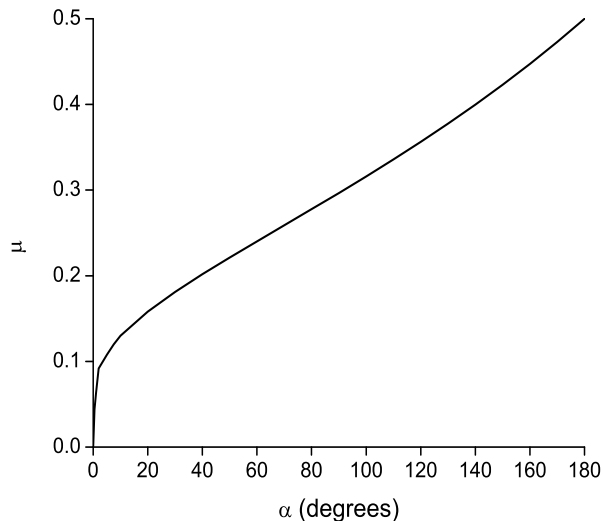
FIG. 12: Relation between the exponent μ and the opening angle α, in the case of diffusion-controlled evaporation from an angular region

the singular property of the reduced pressure function near the contact line (a direct observation is that, due to nonzero value of $\lambda = 1/2$ in the dry-surface evaporation, the order of divergence of $\tilde{\psi}$ is higher by $1/2$ in that case). For the deposition rate in the early time regime, the power law found in the dry-surface evaporation case [6], as well as our result (45), is uniquely determined by the local singular properties of the reduced pressure function at the contact line, and those power law exponents have simple algebraic expressions in terms of μ, λ, and ν.

Both results of Ref. 6 and our results show that the exponent of time t in the power law of deposition rate is independent of the opening angle α in the early time regime, although in our case the deposition process goes slower with exponent 2 instead of $4/3$ in Ref. 6. As regards the dependence on the contact line distance r_0, both results of Ref. 6 and our results (Fig. 9) show that β always remains between -1 and 0 for obtuse opening angles α, and the integrability of the singularity at $r_0 = 0$ holds. As argued in Ref. 6, despite having larger deposition rate, the vertex of the sector does not dominate the sides, and the deposition accumulation at the vertex is not qualitatively different from the deposition accumulation on the sides for obtuse opening angles.

For acute opening angles α, although β remains between -1 and 0 for the dry-surface evaporation, it is constantly -1 in our case. It seems that we have a more concentrated deposition pattern with a nonsingular form of the evaporation rate. The singular flow of the dry-surface evaporation rate J may deflect the streamlines towards the contact line more than in our case, and hence drive

more fluid and mass to the sides and thus away from the apex.[2]

Furthermore, the $1/r_0$ dependence of the deposition rate in the early time regime for acute opening angles seems to violate the integrability and suggests a logarithmic divergence: an arbitrarily large fraction of the mass may accumulate within an arbitrarily small distance from the apex. To resolve this possible singularity, we note that $1/r_0$ dependence occurs not at all times, but only at early times, which are almost never observed near the vertex. Indeed, for each time t one can define a crossover length

$$r^*(t) = \left(t R_i^{\nu-1} \frac{J_0}{\rho} \right)^{1/\nu}. \tag{56}$$

According to the definition of the time scale t_0 (38), the early time condition $t \ll t_0$ corresponds to the condition $r_0 \gg r^*(t)$ in terms of the location of that regime along the contact line. Thus, at each time t, the early time regime is observed only away from the vertex, and the areas near the vertex are always in the intermediate time regime. The natural cutoff $r^*(t)$ actually saves the mass deposition at the tip from being logarithmically infinite.

B. Intermediate time regime

Distinctive power laws characterizing this regime (such as the configuration of the streamlines and the deposition rate) depend on the entire range of φ, including the limit $\varphi \to 0$, which dominates properties of these power laws. An important parameter in this regime is the value of the reduced pressure function at the bisector $\tilde{\psi}(0)$, or the parameter κ^2 (Eq. (32)). Near the bisector, both the evaporation rate J and function $\tilde{\psi}$ are regular, and in order to find $\tilde{\psi}(0)$ one needs to solve the differential equation (19) in the full domain of φ from 0 to $\alpha/2$. Therefore, in the intermediate time regime relevant quantities depend on the functional form of the evaporation rate J and surface shape h in the entire domain of φ and require solution of the main equation (19), in contrast to the early time regime where only the singular behavior at the contact line matters.

The most interesting result in this regime is certainly the qualitatively different behavior of physical quantities in the geometry of the acute opening angles versus obtuse opening angles. Our numerical result for κ^2 (Fig. 6) is not qualitatively different from that found in Ref. 6, as κ^2 changes dramatically at $\alpha = \pi/2$ in both cases.

---

[2] We actually plotted the streamlines for both dry-surface and wet-surface evaporation cases, however, we did not notice any substantial qualitative difference. This result is important and should be provable experimentally, since one should be able to measure mass accumulation at the sides and at the vertex and compare the two evaporation cases.

This is understandable, because the non-smoothness at $\alpha = \pi/2$ is uniquely due to the crossover of the exponent ν in the leading order term determining the surface shape (Eqs. (14) and (15)), while the evaporation rate J behaves smoothly in both cases. However, changes for other quantities that take place at the right opening angle are qualitative in the wet-surface case, unlike in the dry-surface case.

The flow field configuration near the bisector as $\varphi \to 0$, is governed by the exponent ϵ shown in Fig. 7. In the case of dry-surface evaporation, ϵ is larger than 1, except for $\alpha = \pi$, and the streamlines asymptotically diverge from the bisector. In contrast, our wet-surface results show that the streamlines asymptotically converge to the bisector ($\epsilon < 1$) for acute opening angles, while for obtuse opening angles they still diverge. In particular, for the critical angle $\pi/2$ streamlines run parallel to the bisector line, which is not anticipated intuitively.

For the power law of the deposition rate in the intermediate time regime, we obtained the asymptotic form (54). The result for the exponent $\delta(\alpha)$ (Fig. 10) follows the same qualitative pattern as the result in Ref. 6, although it is everywhere larger, so that the deposition process goes slower, like in the early time regime.

For dry-surface evaporation, $\gamma(\alpha)$ remains negative, monotonically increases with α, and becomes 0 at $\alpha = \pi$ (compatible with the symmetry). In the wet-surface evaporation case, $\gamma(\alpha)$ follows a richer pattern. Physically, as γ is strictly larger than -1, the integrability property holds. However, while γ remains negative for obtuse opening angles, it becomes positive for acute angles, and therefore the deposition accumulation is in favor of the sides rather than the vertex as in Ref. 6. In particular, as γ goes to 0 at $\alpha = \pi/2$ and its absolute value remains small nearby, it seems that the wet-surface evaporation case yields a relatively uniform deposition pattern for a wide range of opening angles in the intermediate time regime.

The exponent γ controlling mass deposition is closely related to the trajectory exponent ϵ. From expressions (34) and (53) one can obtain a simple relation:

$$\epsilon = \frac{1}{1+\gamma}, \qquad (57)$$

which is also implicit in Ref. 6. Intuitively, in the intermediate time regime, virtually all the solute between the bisector and the contact line is swept to the contact line and becomes part of the deposit, and therefore γ, the exponent of the contact line distance r_0 indexing the streamlines, should be related to the geometric distribution of the streamlines near the bisector away from the vertex. For $\alpha = \pi$ and $\pi/2$, exponent $\epsilon = 1$, and the streamlines are uniformly distributed near the bisector. Therefore, the solute is uniformly carried to the contact line by the flow, and the deposition rate should be independent of the contact line distance, hence $\gamma = 0$. For other angles, the streamlines become unevenly distributed away from the vertex. When $\epsilon > 1$, they diverge

away from the bisector as $\varphi \to 0$, the smaller contact line distance r_0 is, the nearer the corresponding streamline to the bisector, and more solute will be carried to the spot along the streamline. Therefore the deposition is in favor of the vertex, and γ is negative. When $\epsilon < 1$, γ is positive by the same argument.

To be more precise mathematically, in the intermediate time regime $t_0 \ll t$ the deposition is uniquely determined by the streamline configuration near the bisector line (this is in contrast to the early time regime, where the deposition rate is closely related to the slope of the surface shape near the contact line). The amount of solute deposited near r_0 is controlled by the width of the gap between adjacent streamlines indexed by r_0 and $r_0 + \Delta r_0$ near the bisector line, which is proportional to $r\Delta\varphi$ in the limit $\varphi \to 0$. Near the bisector line, the streamline indexed by r_0 can be expressed as $r \propto r_0 \varphi^{-\epsilon}$ (Eq. (46)). If we consider a small patch $r = const$ near the bisector, and study the intersections of those streamlines with this patch, we have

$$0 = dr \propto \varphi^{-\epsilon} dr_0 - \epsilon r_0 \varphi^{-\epsilon-1} d\varphi, \qquad (58)$$

and therefore

$$\frac{d\varphi}{dr_0} = \frac{\varphi}{\epsilon r_0}. \qquad (59)$$

According to the above argument, Eqs. (46) and (59) yield

$$\frac{dm}{dr_0} \propto \frac{d\varphi}{dr_0} \propto \frac{1}{\epsilon} r_0^{1/\epsilon-1}, \qquad (60)$$

and the relation (57) follows immediately by comparison of the last expression with Eq. (54).

VI. DISCUSSION

The theoretical framework, first established in Ref. 6 and studied here in continuation, captures the essential mechanism of the deposit growth, but does not take into account a number of additional effects that can modify the deposition, and some restrictions and shortcomings remain [6].

The crossover at the opening angle $\alpha = \pi/2$ (as manifested in the surface shape h (13), (14) and (15)), which is certainly independent of the evaporation rate, is quite a subtle point of the theory. As shown in Appendix B, in principle, modifications to the results obtained in this work as well as in Ref. 6 by the asymptotic analysis are needed in the neighborhood of the right opening angle $[\pi/2-\Delta\alpha, \pi/2+\Delta\alpha]$, with $\Delta\alpha \sim (\pi/4) |\ln(r/R_i)|^{-1}$ (Eq. (B9)). The thinner and flatter the drop is, and the closer to the apex, the better our results apply.

Further, we believe the power law exponents obtained by the asymptotic analysis are exact, except for a possible logarithmic modification at $\alpha = \pi/2$, where crossover of exponents could happen. Exact properties of the other

experimentally testable physical quantities (the velocity components, the reduced pressure function $\tilde{\psi}$) in the neighborhood $[\pi/2 - \Delta\alpha, \pi/2 + \Delta\alpha]$ could be in principle interpolated, as shown in Appendix B, since all the physical properties of the system should depend on the opening angle α continuously.

Another interesting observation is the form of the evaporation rate. In this paper, we considered the uniform evaporation, which is simpler than the dry-surface evaporation studied in Ref. 6. The form of the evaporation rate is not arbitrary, and apart from other physical restrictions, it should be compatible with the symmetry of the system. One such consideration would be the following: in the limit $\alpha \rightarrow \pi$ the position of the apex is no longer well defined, and the deposit rate should not depend on the contact line distance r_0 in both early and intermediate time regimes; therefore $\beta(\pi) = \gamma(\pi) = 0$. Combined with the general expression for β (Eq. (61) in Ref. 6), this condition demands

$$\lambda(\pi) + \mu(\pi) = 1, \tag{61}$$

which is satisfied in both cases:[3] for the dry-surface evaporation $\lambda \equiv 1/2$ and $\mu(\pi) = 1/2$, and for the uniform evaporation $\lambda \equiv 0$ and $\mu \equiv 1$. Although $\gamma(\pi) = 0$ in our case, this did not hold exactly for the exponent γ in the dry-surface case, since the approximation of J used for the numerical solution in Ref. 6 was not in exact conformity with the symmetry. In contrast to β, where $\beta(\pi) = 0$ can be traced back to the simple relation (61), the exponent γ is related to the parameter κ^2, which depends on the solution of the main equation (19) in the entire domain of φ. It is interesting to see how the differential equation (19), which is merely a statement of local conservation of mass, together with the proper form of the evaporation rate, yields the deposition properties in full conformity with the symmetry of the system.

In general, various properties of the evaporating drop in the intermediate time regime depend on the mathematical structure over the whole domain of φ, and more thorough analytical treatment of the main equation (19) is certainly appealing. The criticality of the opening angle $\alpha = \pi/2$ demands extra attention: Why do some physical properties differ between acute angle and obtuse angle? Why was not this separation so apparent in Ref. 6, where the same h entered? How is this separation related to the form of the evaporation rate? Naively, these questions can be readily addressed by saying that the criticality of the right angle is uniquely due to the crossover of the leading terms in the full expansion of

the surface shape h at $\alpha = \pi/2$. When the evaporation rate is uniform, it does not introduce any further singularity, and thus helps to retain the trace of the criticality of h in the resulting physical quantities and phenomena. In the case of the dry-surface evaporation, the stronger dependence of J on coordinates may overshadow the coordinate dependence of h, and the latter may appear less significant in the results. In particular, it seems that the change of the exponent μ in the evaporation rate J is in such a direction as to compensate for the change of exponent ν in the surface height h. More mathematically rigorous treatment needs to be done to make this argument clearer.

Experimentally, it is interesting to note some possible applications of our results. Our work shows that wet-surface evaporation at early times with acute opening angle achieves the greatest concentration towards the apex. Accordingly, one could actually achieve a great concentration of mass by allowing the evaporation to occur for a short time, then allowing the dissolved solute to diffuse and equilibrate, then allowing another bit of evaporation, and so forth. In this way, one could approach the behavior of having a finite fraction of the mass within some small distance of the apex. Another interesting aspect is the nearly perfect uniformity of the deposition for the intermediate time regime with opening angle $\alpha \simeq \pi/2$. This kind of uniform deposition may be useful, especially when a small amount of the concentrated substance is sufficient. For example, a dilute solution of reagents can be concentrated strongly at the contact line, thereby inducing a chemical reaction there. The evaporation mechanism assures that the concentration is a known function of the position and the initial dilution. Likewise, trace amounts of solute can be rendered more easily detectable by causing them to concentrate at a contact line.

VII. CONCLUSION

The wet-surface evaporation of an angular drop yields surprisingly rich and potentially useful behavior. This behavior complements the previously studied work on dry-surface evaporation [6]. Though our case lacks the distinctive singular evaporation of the dry-surface evaporation case, remarkably, it leads to a *stronger* focusing of solute towards the apex. Further, it can create two qualitatively different types of flow, according to whether the opening angle is acute or obtuse. The deposition profile is remarkably uniform for the intermediate times when the opening angle is close to a right angle. Now that these deposition properties have been established, they may well prove useful. For example, they provide a means of concentrating trace solutes in a liquid in a rapid and quantitatively predictable way. They also create distinctive capillary flow fields and distinctive concentration profiles of solute. We expect this kind of microscopic, singular, evaporative flow to play an increasing role in the technology of small scale material synthesis, processing and

---

[3] The physical origin of this condition is very simple: for the opening angle $\alpha = \pi$, the evaporation rate should depend only on the normal distance to the contact line $r\sin(\alpha/2 - |\varphi|)$, which reduces to $r(\alpha/2 - |\varphi|)$ when $|\varphi| \rightarrow \alpha/2$. Thus, the exponents of r and $(\alpha/2 - |\varphi|)$ must be equal for this opening angle, and the general expression (55) immediately yields $\mu - 1 = -\lambda$.

analysis.

APPENDIX A: REDUCED PRESSURE EQUATION: OUTER BOUNDARY CONDITION AND REGULARIZATION

In this appendix, we provide a justification of the outer boundary condition (21), and we also show how the boundary problem can be regularized. In Ref. 6, Eq. (19) was solved using the global mass conservation condition

$$\rho \int_{-\alpha/2}^{\alpha/2} |v_r| \, hrd\varphi = \int_0^r \int_{-\alpha/2}^{\alpha/2} J_0 rdrd\varphi, \qquad (A1)$$

where $v_r = h^2 \partial_r \psi$ is the radial component of the flow velocity [6]. However, Eq. (19) in itself is an expression of local mass conservation following Eq. (3). It is therefore interesting to find out explicitly how Eq. (A1) represents new information that can restrict the solution. Here we explain the origin of the new information and show that it takes the form of an explicit boundary condition.

With the expressions of h and ψ, Eq. (A1) can be simplified as

$$\int_0^{\alpha/2} \left(2 \left(3\nu - 2 \right) \tilde{h}^3 \tilde{\psi} - 1 \right) d\varphi = 0. \qquad (A2)$$

The local mass conservation implicitly stated in Eq. (19) allows us to express $\tilde{\psi}$ in terms of the derivative $d\tilde{\psi}/d\varphi$:

$$2(3\nu - 2)\tilde{\psi}\tilde{h}^3 = \tilde{h}^3 \frac{d^2\tilde{\psi}}{d\varphi^2} + 3\tilde{h}^2 \frac{d\tilde{h}}{d\varphi}\frac{d\tilde{\psi}}{d\varphi} + 1. \qquad (A3)$$

Then integration by parts, together with the boundary condition (20), converts the integral condition (A2) into the boundary condition (21).

We now show that condition (21) does in fact restrict the general form of $\tilde{\psi}$ and fixes the order of its divergence near the contact line. To demonstrate this, we study the asymptotic behavior of $\tilde{\psi}$. As both $\tilde{h}$ and $\tilde{\psi}$ are even in φ, we can consider only the domain $0 \leq \varphi \leq \alpha/2$. We restrict our attention to the limit $\varphi \to \alpha/2$ and keep in mind that $\tilde{h} \propto (\alpha/2 - \varphi)$ in this limit. From the expressions of $\tilde{h}$ (14) and (15), as well as Eq. (19), we see that $\tilde{\psi}$ necessarily diverges in this limit, and the third term on the left side of Eq. (19), which is of the lowest order of divergence, can be neglected in the asymptotic analysis. Thus, Eq. (19) reduces to:

$$\frac{d^2\tilde{\psi}}{d\varphi^2} + \frac{3}{\tilde{h}}\frac{d\tilde{h}}{d\varphi}\frac{d\tilde{\psi}}{d\varphi} + \frac{1}{\tilde{h}^3} = 0. \qquad (A4)$$

Eq. (A4) can be solved analytically. First, consider the homogeneous first order differential equation for $d\tilde{\psi}/d\varphi$:

$$\frac{d}{d\varphi}\left(\frac{d\tilde{\psi}}{d\varphi} \right) + \frac{3}{\tilde{h}}\frac{d\tilde{h}}{d\varphi}\frac{d\tilde{\psi}}{d\varphi} = 0, \qquad (A5)$$

which has the general solution of the form:

$$\frac{d\tilde{\psi}}{d\varphi} = c\frac{1}{\tilde{h}^3}, \qquad (A6)$$

with c being an arbitrary constant. In order to obtain the general solution of the inhomogeneous equation (A4), we let c be a function of φ, i.e., $d\tilde{\psi}/d\varphi = c(\varphi)/\tilde{h}^3$, then plug it into Eq. (A4) and find

$$\frac{dc}{d\varphi} = -1, \qquad (A7)$$

which means

$$c(\varphi) = -\varphi + const. \qquad (A8)$$

Combining Eqs. (A6) and (A8), we find that Eq. (A4) has a general solution of the form:

$$\tilde{\psi} \to C_1 + C_2 \int_0^\varphi \frac{d\xi}{\tilde{h}^3(\xi)} - \int_0^\varphi \frac{\xi}{\tilde{h}^3(\xi)}d\xi, \qquad \varphi \to \frac{\alpha}{2}, \qquad (A9)$$

where C_1 and C_2 are arbitrary constants. We can display the divergence of $\tilde{\psi}$ in this limit more explicitly by expanding the right-hand side of Eq. (A9) in terms of $(\alpha/2 - \varphi)$:

$$\tilde{\psi} \to \frac{1}{2}\left(C_2 - \frac{\alpha}{2} \right)\left| \frac{d\tilde{h}}{d\varphi}\left(\frac{\alpha}{2} \right) \right|^{-3}\left(\frac{\alpha}{2} - \varphi \right)^{-2}$$
$$+ \left| \frac{d\tilde{h}}{d\varphi}\left(\frac{\alpha}{2} \right) \right|^{-3}\left(\frac{\alpha}{2} - \varphi \right)^{-1} + const, \qquad (A10)$$

where we only retained the divergent terms and the constant term, and accordingly,

$$\frac{d\tilde{\psi}}{d\varphi} \to \left(C_2 - \frac{\alpha}{2} \right)\left| \frac{d\tilde{h}}{d\varphi}\left(\frac{\alpha}{2} \right) \right|^{-3}\left(\frac{\alpha}{2} - \varphi \right)^{-3}$$
$$+ \left| \frac{d\tilde{h}}{d\varphi}\left(\frac{\alpha}{2} \right) \right|^{-3}\left(\frac{\alpha}{2} - \varphi \right)^{-2}. \qquad (A11)$$

Now it becomes immediately apparent that condition (21) demands $C_2 = \alpha/2$, and only the first order divergence of $\tilde{\psi}$ is allowed (which is always present, as is clear from Eq. (A10)).

On reflection, the physical content associated with the boundary condition (21) may invite further exposition. Taking into account Eqs. (9) and (10), we note that the boundary condition (21) states physically $h\mathbf{v} = 0$ at the contact line. Consider a region within distance δ from

the boundary. The influx $h\mathbf{v}$ should be balanced with the evaporation flux, which is proportional to $J\delta$. Let δ go to 0, and our result follows. Mathematically, one can argue that singular behavior of Eq. (19) and the order of divergence of $\tilde{\psi}$ in the limit $\varphi \to \alpha/2$ are uniquely determined by the term $1/\tilde{h}^3$. The solution with a higher-order divergence, though compatible with the mathematical structure, is not allowed by the physics.

To make the boundary condition (21) easier to handle mathematically, we define a regularized function:

$$\tilde{\chi} = \tilde{h}^2 \tilde{\psi}, \qquad (A12)$$

where $\tilde{h}^2$ is introduced to compensate for the second order divergence in $\tilde{\psi}$ at the contact line allowed by Eq. (19). The original problem is converted to the standard boundary value problem:

$$\tilde{h}\frac{d^2\tilde{\chi}}{d\varphi^2} - \frac{d\tilde{h}}{d\varphi}\frac{d\tilde{\chi}}{d\varphi} - \left(2\frac{d^2\tilde{h}}{d\varphi^2} + 2(3\nu - 2)\tilde{h}\right)\tilde{\chi} = -1, \; (A13)$$

$$\left.\frac{d\tilde{\chi}}{d\varphi}\right|_{\varphi=0} = 0, \qquad \chi\left(\frac{\alpha}{2}\right) = 0,$$

where $\tilde{\chi}$ is defined in the domain $-\alpha/2 \le \varphi \le \alpha/2$ and is even in φ. The boundary problem (A13) has a unique solution, which we plot in Fig. 4 for two opening angles ($\alpha = \pi/4$ and $3\pi/4$).

The introduction of the regularized pressure function $\tilde{\chi}$ is not special to the uniform evaporation case, and it could be readily defined with a more general and singular evaporation profile. Function $\tilde{h}$ in Eq. (A12) is independent of the evaporation, and its exponent 2 is introduced to compensate for the possible singularity of the reduced pressure function $\tilde{\psi}$ in the uniform evaporation case. With a more general evaporation rate, singular behavior of $\tilde{\psi}$ may depend on the singularity of the evaporation rate, and the exponent of $\tilde{h}$ in the definition (A12) should be adjusted accordingly. It can be shown that in the case of the dry-surface evaporation the exponent becomes $5/2$ due to the divergence of the evaporation rate at the contact line.

We use both functions $\tilde{\psi}$ and $\tilde{\chi}$ in this paper. Function $\tilde{\chi}$ is employed to obtain the numerical results because of its regularity, and function $\tilde{\psi}$ is used in asymptotic analysis because of its simple asymptotic form and its direct connection to the physical properties of the system and their singular behavior.

APPENDIX B: CROSSOVER AT THE 90-DEGREE OPENING ANGLE

It has been shown [5, 17] that in the limit $r \ll R(t) \approx R_i$ the first two leading order terms in the full expansion of the surface height $h(t, r, \varphi)$ read: for the opening angle α in the vicinity of $\pi/2$, but not strictly equal to $\pi/2$:

$$h(r, \varphi) = \frac{1}{4}\frac{r^2}{R_i}\left(\frac{\cos 2\varphi}{\cos \alpha} - 1\right) + C(\alpha)\frac{r^{\pi/\alpha}}{R_i^{\pi/\alpha-1}}\cos\frac{\pi\varphi}{\alpha}, \tag{B1}$$

and at exactly $\alpha = \pi/2$:

$$h(r, \varphi) = -\frac{1}{\pi}\frac{r^2}{R_i}\ln\frac{r}{R_i}\cos 2\varphi$$
$$+ \frac{r^2}{R_i}\left(\frac{1}{\pi}\varphi\sin 2\varphi - \frac{1}{4} + C_0 \cos 2\varphi\right), \tag{B2}$$

where $C(\alpha)$ and C_0 are related by Eq. (16), and C_0 is independent of α. For simplicity, we replaced $R(t)$ with R_i and hence suppressed the time dependence of h.

As mentioned before, the apparent divergence in Eqs. (14), (15), and hence (B1) at $\alpha = \pi/2$ is artificial, and, as an implicit function of α, the surface shape $h(r, \varphi)$ is actually continuous at $\alpha = \pi/2$. This can be readily checked by expanding the divergent terms in small parameter $(\pi/2 - \alpha)$ near $\alpha = \pi/2$ as was done in Refs. 5 and 17. Moreover, as can be shown by the same method, all the derivatives of h with respect to r and φ up to any order are also continuous at $\alpha = \pi/2$.

We can actually estimate the size of the neighborhood $[\pi/2 - \Delta\alpha, \pi/2 + \Delta\alpha]$ where the first and the second leading order terms on the right side of Eq. (B1) are comparable to each other by comparing the dominant divergent terms in expressions (B1) and (B2). For $\alpha < \pi/2$, $\alpha = \pi/2 - \Delta\alpha$, we have

$$\frac{1}{4}\frac{r^2}{R_i}\frac{\cos 2\varphi}{\cos \alpha} \sim -\frac{1}{\pi}\frac{r^2}{R_i}\ln\frac{r}{R_i}\cos 2\varphi, \tag{B3}$$

or, since $\cos \alpha \approx \Delta\alpha$,

$$\Delta\alpha \sim \frac{\pi}{4}\left|\ln\frac{r}{R_i}\right|^{-1}. \tag{B4}$$

For $\alpha > \pi/2$, $\alpha = \pi/2 + \Delta\alpha$, and with $C(\alpha)$ given by Eq. (16), one can easily obtain:

$$\frac{1}{4\Delta\alpha}\frac{r^{\pi/\alpha}}{R_i^{\pi/\alpha-1}}\cos 2\varphi \sim -\frac{1}{\pi}\frac{r^2}{R_i}\ln\frac{r}{R_i}\cos 2\varphi, \tag{B5}$$

or, since $(r/R_i)^{\pi/\alpha-2} \approx (r/R_i)^{-4\Delta\alpha/\pi}$,

$$\Delta\alpha \sim \frac{\pi}{4}\left|\ln\frac{r}{R_i}\right|^{-1}\left(\frac{r}{R_i}\right)^{-4\Delta\alpha/\pi}. \tag{B6}$$

Since $\Delta\alpha$ is always small whenever $r \ll R_i$, the estimates (B4) and (B6) actually provide compatible results.

In asymptotic analysis employed in this paper as well as in Ref. 6, only the term of the smaller exponent of r ($\pi/\alpha \lessgtr 2$ according to $\alpha \gtrless \pi/2$) was retained on the right side of Eq. (B1), treating $\alpha = \pi/2$ as the limiting case despite a crossover of the exponents at this value. This approximation does bring about some subtleties on some

occasions, and necessary corrections or modifications of our results need to be made. Moreover, although the existence of the crossover region $[\pi/2 - \Delta\alpha, \pi/2 + \Delta\alpha]$ is uniquely due to the asymptotic form of surface shape h, it does manifest itself in other properties of the evaporating drop. It is interesting to see how the crossover affects our asymptotic analysis of the system.

In the case of the velocity field, it was found in Eq. (29) that v_φ at the contact line would vanish in the limit $\alpha \to \pi/2$. However, intuitively, according to the conservation of the fluid mass, locally the velocity should be inversely proportional to the slope of the surface of the drop. As mentioned above, $\partial h/\partial\varphi$ remains finite and depends continuously on the opening angle, even at $\alpha = \pi/2$, and therefore $v_\varphi|_{\alpha=\pi/2}$ should not be vanishing as well. Indeed, if, instead of employing Eqs. (14) and (15), we use the leading order term $h(r,\varphi)|_{\alpha=\pi/2} = -(1/\pi)(r^2/R_i)\ln(r/R_i)\cos 2\varphi$ on the right-hand side of Eq. (B2) in Eq. (28) and let $\nu = 2$, we obtain:

$$ v_\varphi|_{\alpha=\pi/2} \to \frac{J_0}{\rho}\frac{\pi}{2}\left(\frac{r}{R_i}\right)^{-1}\left|\ln\frac{r}{R_i}\right|^{-1}, \qquad \text{(B7)} $$

which is non-vanishing at the contact line.

Combining Eqs. (29) and (B7), we can again identify a crossover region near the opening angle $\alpha = \pi/2$, which was somewhat concealed by the asymptotic analysis we

employed in this paper as well as in Ref. 6. We believe, as partly shown above, that the velocity field (as well as all other physical properties of the system) depends on the opening angle α continuously. And in the small neighborhood $[\pi/2 - \Delta\alpha, \pi/2 + \Delta\alpha]$ actual physical properties should be interpolated, so that Eq. (29), which holds only outside of this neighborhood, is related continuously to the result (B7), which applies exactly at $\alpha = \pi/2$. By comparing Eqs. (29) and (B7), we see that

$$ \tan\left(\frac{\pi}{2} - \Delta\alpha\right) \sim \frac{4}{\pi}\left|\ln\frac{r}{R_i}\right|, \qquad \text{(B8)} $$

and therefore we can find an estimate for $\Delta\alpha$:

$$ \Delta\alpha \sim \frac{\pi}{2} - \arctan\frac{4}{\pi}\left|\ln\frac{r}{R_i}\right| \approx \frac{\pi}{4}\left|\ln\frac{r}{R_i}\right|^{-1}. \qquad \text{(B9)} $$

Result (B9) is identical to Eq. (B4). To no surprise, the crossover originating from the surface was recovered in the result for the velocity, which was determined using that surface shape. Similar interpolative estimates can be conducted for all other physical quantities. In principle, all the results we obtained so far (as well as those in Ref. 6) apply only outside of the neighborhood $[\pi/2 - \Delta\alpha, \pi/2 + \Delta\alpha]$.

[1] R. D. Deegan, O. Bakajin, T. F. Dupont, G. Huber, S. R. Nagel, T. A. Witten, *Nature,* **389,** 827 (1997).
[2] R. D. Deegan, *Ph.D. Thesis* (University of Chicago, Dept. of Physics, 1998).
[3] R. D. Deegan, O. Bakajin, T. F. Dupont, G. Huber, S. R. Nagel, T. A. Witten, *Phys. Rev. E* **62**, 756 (2000).
[4] R. D. Deegan, *Phys. Rev. E* **61**, 475 (2000).
[5] Y. O. Popov, T. A. Witten, *Eur. Phys. J. E* **6**, 211 (2001).
[6] Y. O. Popov, T. A. Witten, *Phys. Rev. E* **68**, 036306 (2003).
[7] Y. O. Popov, *Ph.D. Thesis* (University of Chicago, Dept. of Physics, 2003).
[8] Y. O. Popov, *Phys. Rev. E* **71**, 036313 (2005).
[9] N. D. Denkov, O. D. Velev, P. A. Kralchevsky, I. B. Ivanov, H. Yoshimura, K. Nagayama, *Langmuir* **8**, 3183 (1992).
[10] A. S. Dimitrov, C. D. Dushkin, H. Yoshimura, K. Nagayama, *Langmuir* **10**, 432 (1994).
[11] T. Ondarcuhu, C. Joachim, *Europhys. Lett.* **42**, 215 (1998).
[12] J. Boneberg, F. Burmeister, C. Shafle, P. Leiderer, D. Reim, A. Fery, S. Herminghaus, *Langmuir* **13**, 7080 (1997).
[13] R. G. Larson, T. T. Perkins, D. E. Smith, S. Chu, *Phys. Rev. E* **55**, 1794 (1997).
[14] O. B. Bakajin, T. A. J. Duke, C. F. Chou, S. S. Chan, R. H. Austin, E. C. Cox, *Phys. Rev. Lett.* **80**, 2737 (1998).
[15] C. C. Hsieh, L. Li, R. G. Larson, *J. Non-Newtonian Fluid Mech.* **113**, 147 (2003).
[16] Y. O. Popov, *J. Colloid and Interface Sci.* **252**, 320 (2002).
[17] H. K. Moffat, B. R. Duffy, *J. Fluid. Mech.* **96**, 299 (1979).
[18] S. Blume, M. Kirchner, *Optik* **29**, 185 (1969).